Design of a Crossflow Attenuated Natural Laminar Flow Flight Test Article

Michelle N. Lynde[1], Richard L. Campbell[2], Brett R. Hiller[3], and Lewis R. Owens[4]
NASA Langley Research Center, Hampton, Virginia, 23681, USA

A natural laminar flow test article has been designed and analyzed for a flight test at the NASA Armstrong Flight Research Center using the F-15 aircraft with Centerline Instrument Pylon (CLIP) testbed. The flight test aims to experimentally validate the new Crossflow Attenuated Natural Laminar Flow (CATNLF) design method in a flight environment. The CATNLF design method uses geometry shaping to produce specific pressure distributions that enable laminar flow on vehicle components with high sweep and high Reynolds numbers by attenuating the crossflow growth that typically leads to premature transition on such components. The CATNLF test article, which will be mounted vertically below the F-15 for flight testing, is designed to be representative of a transonic transport wing and accounts for transition mechanisms due to crossflow, Tollmien-Schlichting, and attachment line transition instabilities. The test article is predicted to support 53% surface area of laminar flow on the suction-side at the design point and maintains significant laminar flow extents at near-cruise, off-design conditions. The design was performed, flight matrix selected, and instrumentation chosen with two primary test goals in mind: to confirm the effectiveness of the CATNLF method in attenuating crossflow growth on a representative transonic transport wing, and to investigate surface requirements needed for laminar flow applications.

Nomenclature

Acronyms

BLSTA3D	=	Boundary Layer code for Stability Analysis 3D, boundary layer profile solver
CATNLF	=	Crossflow Attenuated Natural Laminar Flow
CDISC	=	Constrained Direct Iterative Surface Curvature, design module
CF	=	Crossflow
CLIP	=	Centerline Instrument Pylon
CRM-NLF	=	Common Research Model with Natural Laminar Flow
DRE	=	Distributed Roughness Elements
FC	=	Full Configuration
FCDB	=	Full Configuration Design Box
ITA	=	Isolated Test Article
LASTRAC	=	Langley Stability and Transition Analysis Code, transition prediction software
LFC	=	Laminar Flow Control
LST	=	Linear Stability Theory
NASA	=	National Aeronautics and Space Administration
NLF	=	Natural Laminar Flow
NTF	=	National Transonic Facility
RANS	=	Reynolds-Averaged Navier-Stokes
ReHEAT	=	Resistive Heating for the Evaluation of Aerodynamic Transition
SWLF	=	Swept-Wing Laminar Flow
TS	=	Tollmien-Schlichting
USM3D	=	Unstructured Mesh 3D, Navier-Stokes flow solver

[1] Research Aerospace Engineer, Configuration Aerodynamics Branch, AIAA Member.
[2] Senior Research Engineer, Configuration Aerodynamics Branch, AIAA Associate Fellow.
[3] Research Aerospace Engineer, Configuration Aerodynamics Branch, AIAA Member.
[4] Senior Research Engineer, Flow Physics and Control Branch, AIAA Senior Member.

Symbols

$\alpha_{F\text{-}15}$	=	Angle of attack of the F-15
α_{ITA}	=	Angle of attack for the isolated test article grid
$\beta_{F\text{-}15}$	=	Angle of sideslip of the F-15
β_{FC}	=	Angle of sideslip for the full configuration grid
c	=	Chord length
c_l	=	Sectional lift coefficient
C_P	=	Pressure coefficient
deg	=	Degree
ft	=	Foot
η	=	Span location nondimensionalized by test article span
in	=	Inch
M	=	Mach number
Re_c	=	Reynolds number based on local chord
Re_{MAC}	=	Reynolds number based on mean aerodynamic chord
Re_θ	=	Reynolds number based on attachment line boundary layer momentum thickness
Re'	=	Unit Reynolds number
x/c	=	x-location nondimensionalized by local chord
z/c	=	z-location nondimensionalized by local chord

I. Introduction

AVIATION has developed into a strong industry over the last century, with particularly rapid growth over the previous few decades due in part to a booming commercial market and increased demand for air cargo capabilities. Current market projections suggest air traffic will continue to grow by approximately 4.6% over the next 20 years, inspiring the aviation industry to develop next-generation aircraft to accommodate this anticipated growth [1]. Increased environmental awareness has led to ambitious performance goals for these next-generation aircraft in order to make the projected air travel demands compatible with new ecofriendly regulations. Objectives for Green Aviation, including increased fuel efficiency, lower emissions, and reduced noise, have motivated technological research and development of promising concepts that may help reach these performance goals. One such technology being investigated is the implementation of laminar flow, which offers the potential to increase fuel efficiency by significantly reducing aircraft drag via lower skin friction and profile drag. Laminar flow technology has been researched since the 1940s with various successful, yet limited, applications. Recently, laminar flow has begun making its way onto modern commercial aircraft on components such as the nacelles, winglets, fuselage, and low-swept wings [2, 3]. While these existing applications of laminar flow have proven to reduce aircraft drag, one of the greatest performance improvement opportunities using laminar flow is its implementation on the wings of typical commercial transports. The main wings have been a challenge for applications of laminar flow primarily due to the rapid growth of crossflow instabilities that occurs on components with high sweep (greater than 25 deg) or Reynolds numbers (greater than 25 million). Most modern commercial transports have highly swept wings in order to meet cruise speed requirements. Historic techniques to address transition due to crossflow instabilities include a laminar flow control (LFC) system or a reduction in wing sweep. LFC systems, such as suction, often increase the complexity, cost, and weight of the vehicle, which has limited the application of LFC systems on commercial transports. A reduction in wing sweep inherently requires an often undesirable reduction in the cruise speed of the vehicle. A more recent technology, distributed roughness elements (DREs), has demonstrated some success in reducing crossflow instabilities, but inconsistent flight test results have required additional fundamental research before any commercial application is feasible [4].

A new laminar flow technology, referred to as Crossflow Attenuated Natural Laminar Flow (CATNLF), has been developed to reduce the growth of crossflow instabilities on components with high sweep and high Reynolds numbers. The CATNLF method utilizes airfoil geometry shaping to obtain specific pressure distributions that are known to reduce crossflow growth to a subcritical level in the leading-edge region of a wing. This method has been applied in computational studies to both transonic and supersonic commercial transports [5, 6]. The CATNLF method was employed in the design of a wind tunnel model, referred to as the Common Research Model with Natural Laminar Flow (CRM-NLF), which was tested in the National Transonic Facility (NTF) at the NASA Langley Research Center to experimentally validate the computational predictions of the technology [7]. Experimental results from the wind tunnel test showed significant extents of laminar flow at transonic cruise speeds, as well as good agreement between the experimental data and computational predictions of laminar flow regions [8, 9, 10]. The successful wind tunnel

test has led to the use of the CRM-NLF model as the primary test configuration in the AIAA Transition Prediction Workshop, highlighting the current industry interest in practical laminar flow applications. Figure 1 compares the maximum extent of laminar flow, measured in maximum transition Reynolds number, for a variety of natural laminar flow (NLF) experiments (blue circles) originally compiled by Malik et al. [11]. A line has been added to the data to signify a notional boundary for components that could support NLF using classical methods. The gray band of sweeps from 34 to 38 deg highlights the components of interest for this research, representing sweeps seen on modern transonic transports with a cruise Mach number of approximately 0.85. This plot illustrates the relatively large extents of laminar flow seen on the CRM-NLF in the NTF compared to historic NLF experiments on components with comparable sweep, alluding to the success of the CATNLF method in reducing the crossflow growth on highly swept wings.

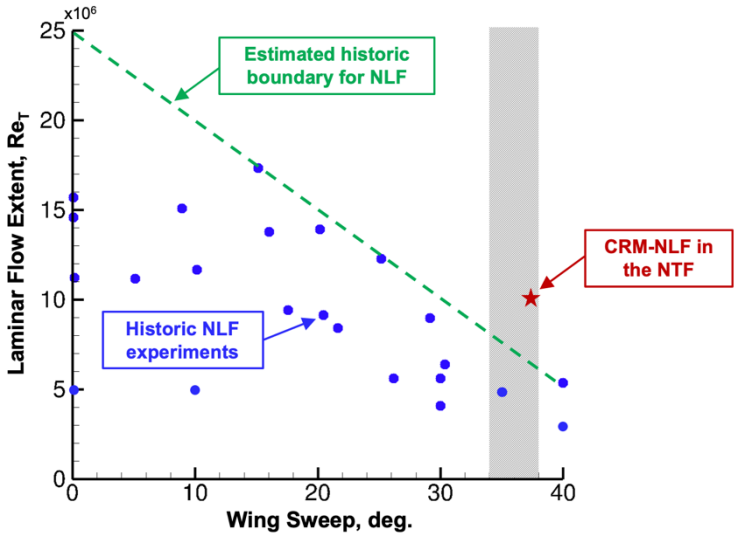

Figure 1. Data originally compiled by Malik et al. [11] that compare extents of laminar flow seen on several NLF experiments. Some additional data representing current production aircraft, a notional NLF boundary, and the CRM-NLF test in the NTF are added to the original data. The gray band highlights sweeps of interest for this research.

While the CRM-NLF wind tunnel test in the NTF provided preliminary experimental confirmation of the CATNLF technology, challenges during the experimental investigation limited the test conditions at which high-quality data could be acquired. Extents of laminar flow are strongly dependent on environmental factors, such as freestream turbulence levels, and can be limited by bypass transition due to surface imperfections. These environmental factors and bypass transition are typically more detrimental to the extent of laminar flow in a wind tunnel environment compared to a flight environment. This is primarily because the freestream turbulence levels are usually higher in a wind tunnel, which results in a lower critical N-factor and causes earlier boundary layer instability transition. Additionally, the model size restrictions in a wind tunnel requires increased unit Reynolds numbers to obtain the desired chord Reynolds numbers in cryogenic facilities like the NTF. These increased unit Reynolds numbers thin the boundary layer and make smaller surface imperfections critical, leading to additional bypass transition in the wind tunnel. During the CRM-NLF test in the NTF, the extents of laminar flow at the high Reynolds number test conditions (i.e., $Re_{MAC} > 20$ million) were limited by bypass transition. This high Reynolds number limitation led to the proposal of a flight test series to experimentally validate the CATNLF method in a flight environment, which includes lower turbulence levels, as well as lower unit Reynolds numbers than those seen in the NTF for the same chord Reynolds numbers because of an increased model size in flight. The upcoming flight test series is a collaborative effort between researchers and engineers at the NASA Langley Research Center and the NASA Armstrong Flight Research Center. It is comprised of three flight tests, all of which will be flown on an existing flight testbed at the Armstrong Flight Research Center known as the Centerline Instrument Pylon (CLIP) underneath an F-15 aircraft. This flight testbed has been successfully used for previous laminar flow experiments [12]. The first of three flight tests in the series, referred to as Resistive Heating for the Evaluation of Aerodynamic Transition (ReHEAT), is to validate an experimental test technique that will improve the efficiency and quality of the laminar flow visualization data acquired during the flight test series. ReHEAT was successfully completed in 2019 and some results from the flight test have been published by Watkins et al. [13]. The second flight test, referred to as Flow Rake, will gather essential information about the flow

quality beneath the F-15, including local conditions and turbulence levels, and is scheduled to fly in 2022. The final flight test, referred to as CATNLF, will be used to evaluate the CATNLF technology in a flight-relevant environment and is the subject of the present paper. The test article used in the final flight test has been designed using the CATNLF method to delay transition at transonic cruise speeds on high sweep, high Reynolds number components. The CATNLF test article is planned to be used to accomplish two primary goals: first, to confirm the effectiveness of the CATNLF method in attenuating crossflow growth at conditions representative of a modern transonic transport wing, and second, to investigate surface requirements needed for laminar flow applications.

This paper documents the computational design and analysis of the CATNLF flight test article, including information on the computational tools, transition delay method, test article airfoil geometry and pressure, and predicted extents of laminar flow. The paper also provides an overview of the flight test strategy, test article instrumentation, and computational results for several planned test conditions. The test article is scheduled to be manufactured in 2021 with flight testing tentatively beginning in 2022.

II. Design and Analysis Approach

The aerodynamic design of the CATNLF flight test article was performed using a suite of computational tools with the goal of obtaining significant extents of laminar flow at the cruise design condition. This subsection will present the computational tools employed in the design and analysis process, as well as a brief description of the CATNLF boundary layer transition delay method.

A. Computational Tools

Several computational tools were used during the aerodynamic design and analysis of the CATNLF test article, including a flow solver, design code, and transition prediction software. The work flow of the computational tools is illustrated in Figure 2. The flow solver chosen for this work, USM3D [14], is a Reynolds-averaged Navier-Stokes (RANS) solver that uses unstructured tetrahedral grids. A variety of grids were developed for this work, which are described in the following section. All flow solutions were obtained using the Spalart-Allmaras turbulence model, and powered-engine boundary conditions were used in solutions with the full aircraft modeled. This flow solver was coupled with the design code to determine the shape of the test article. The design code used is a knowledge-based inverse design tool, CDISC [15], which has been used in many aerodynamic design projects including computational studies, wind tunnel models, and flight test efforts. CDISC works by iteratively creating target pressure distributions, comparing the target and current analysis pressure distributions, then adjusting the geometry to better match the target pressures. The CDISC target pressure architecture used in this work is described in the following subsection. For transition prediction, a boundary layer profile solver, BLSTA3D [16], was used to calculate the velocity and temperature profiles from the flow solver chordwise pressure distributions. These boundary layer profiles are used in LASTRAC [17], the stability analysis code, to calculate the growth of both Tollmien-Schlichting (TS) and crossflow (CF) modal instabilities and estimate the extents of laminar flow on the flight test article. All stability analysis calculations use the e^N method based on Linear Stability Theory (LST) with compressibility effects included and no curvature effects. For the flight environment, a critical N-factor of 10 is used for both TS and CF instabilities to predict the location of transition.

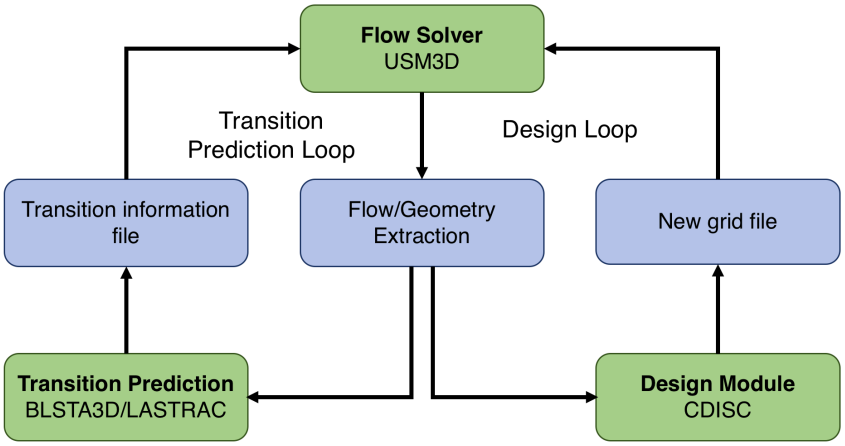

Figure 2. Flow chart for the computational tools employed in this aerodynamic design work.

B. Crossflow Attenuated Natural Laminar Flow (CATNLF) Design Method

The CATNLF transition delay method aims to enable significant extents of laminar flow on wings with high sweep and high Reynolds number, such as those on traditional transonic transports, that have previously been limited by crossflow transition. The strategy used to suppress the crossflow growth in the leading-edge region, as well as control the midchord Tollmien-Schlichting transition location, is to introduce a unique pressure distribution architecture. The CATNLF method of transition delay was developed in computational studies [6, 7, 18] and experimentally investigated in a wind tunnel test in 2018 [7, 8, 9, 10].

A sample CATNLF pressure distribution for a transonic wing is shown in Figure 3 with several key features highlighted. The rapid acceleration near the leading edge is the primary mechanism for keeping the crossflow growth subcritical. A pressure gradient tailored to control Tollmien-Schlichting growth is introduced between the end of the rapid acceleration region and the desired chordwise transition location. Figure 4 shows the CF and TS N-factor growth associated with the sample CATNLF pressure distribution from Figure 3 at a chord Reynolds number of 40 million. The characteristics shown in the N-factor growth plots are representative of those seen on typical CATNLF wings. The CF grows rapidly over a short region near the leading edge, reaches a subcritical maximum value, and then damps over the remainder of the chord. The TS growth is designed to slowly increase from the leading edge to the desired chordwise transition location. These N-factor growth plots show that CATNLF pressure distributions are expected to transition due to TS in the midchord region forward of the shock at the design condition. This CATNLF strategy for controlling transition will be implemented on the test article.

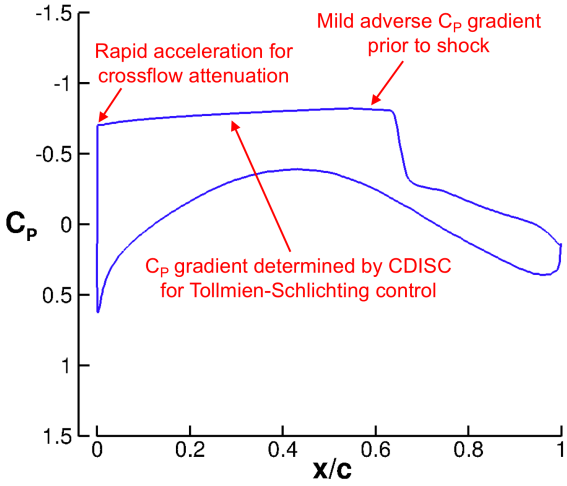

Figure 3. Sample CATNLF pressure distribution for a typical transonic transport with several key features labeled.

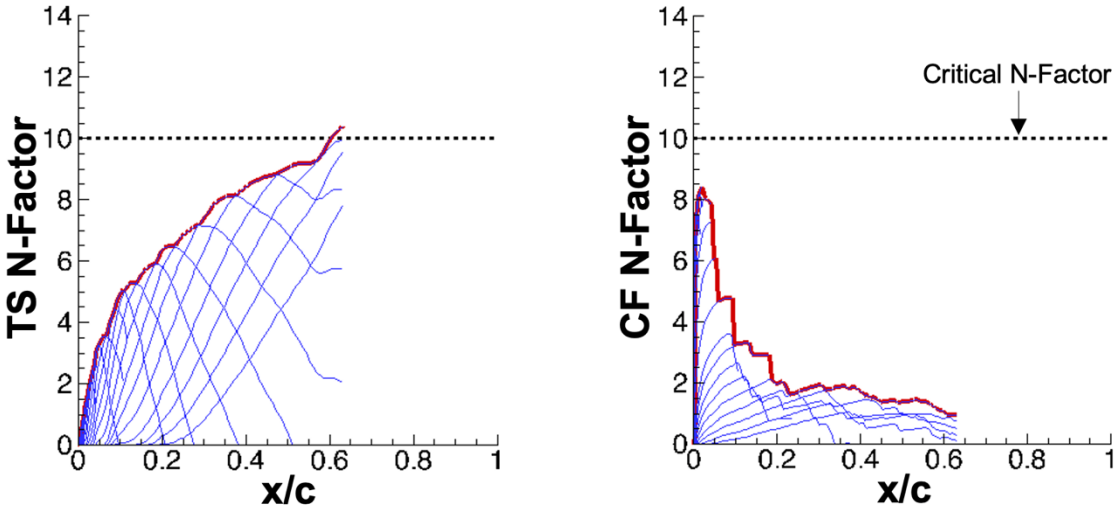

Figure 4. N-factor growth for both TS (left) and CF (right) for the sample CATNLF pressure distribution seen in Figure 3 at 40 million chord Reynolds number.

III. CATNLF Flight Test Article Design Approach and Results

The primary goal of the flight test effort is to experimentally investigate the CATNLF transition delay method in a flight environment. The test article has been computationally designed using the tools and methods described previously. This section will cover the results of the design, including airfoil shapes, pressure distributions, and predicted extents of laminar flow. This section also includes computations for off-design conditions to evaluate the robustness of the transition delay method in representative near-cruise flight conditions.

A. Design Approach

The CATNLF flight test article was designed to be as representative as possible of a typical transonic transport wing, which motivated the test article geometry and design conditions selected for this work. As mentioned, the test article will be flown attached to the CLIP underneath an F-15 aircraft, as shown in Figure 5. The CATNLF test article was sized to have a leading-edge sweep of 35 deg and to maximize the test article chord length subject to mounting restrictions and ground clearance requirements. The baseline planform geometry is shown in Figure 6 with reference parameters listed in Table 1. The design flight condition was chosen based on the F-15 flying at an altitude of 5,000 ft at Mach 0.85. This flight condition creates a Reynolds number based on mean aerodynamic chord of 31 million on the test article at the design point. The CATNLF test article is designed to be loaded similar to a transonic transport, with a sectional lift coefficient targeted around 0.5. Laminar flow is only targeted for the suction side on this test article.

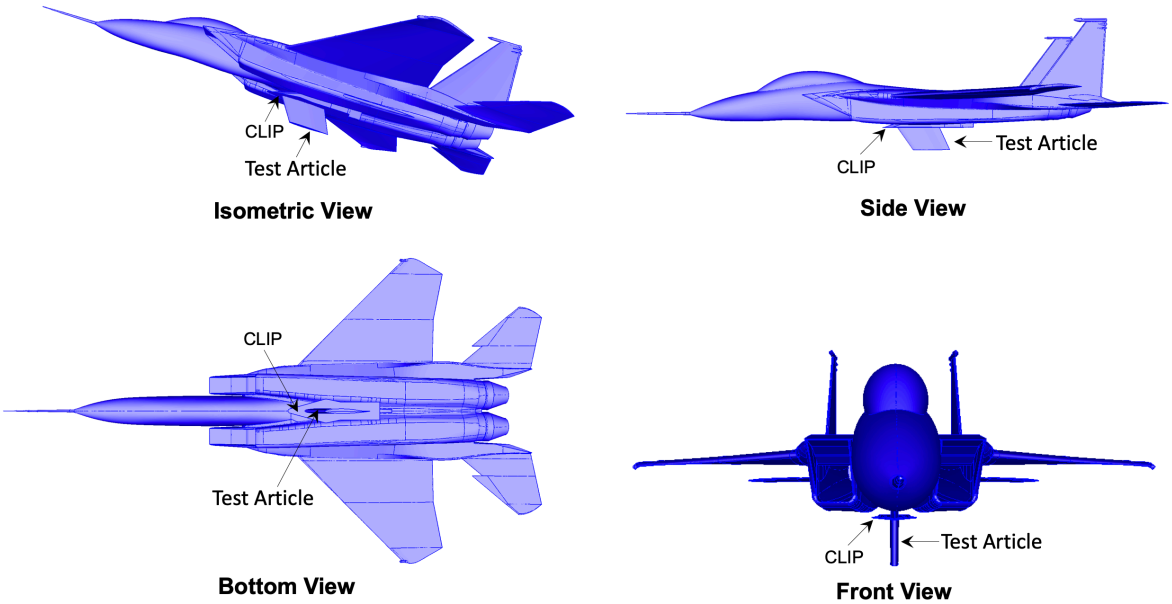

Figure 5. Flight test configuration showing the test article attached to the bottom of the F-15 via the CLIP.

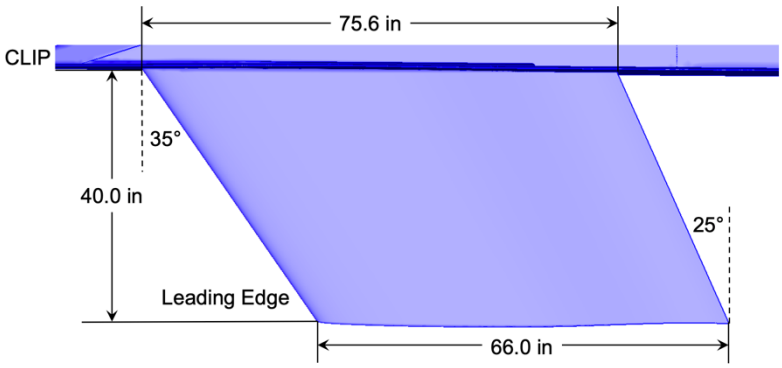

Figure 6. Test article baseline planform shape with dimensions.

Table 1. Reference parameters and design flight conditions for the CATNLF test article.

Mean Aerodynamic Chord	5.9 ft (70.8 in)
Span	3.3 ft (40.0 in)
Reference Area	19.7 ft^2 (2836.8 in^2)
Leading-edge Sweep	35 deg
Trailing-edge Sweep	25 deg
Max Thickness	10% chord
Design Mach	0.85
Design Sectional Lift	0.50
Design Altitude	5,000 ft
Design Re_{MAC}	31.0×10^6
Design Re'	5.3×10^6 /ft
Design Critical N-factor	10

Due to the complexity of the F-15 and CLIP geometry, it was advantageous to simplify the modeled configuration to reduce computational time and resources needed for the design of the flight test article. Three flow solver grids were utilized for this work to allow for a more efficient design process. The first grid modeled the entire configuration that will be tested in flight, including the fullspan F-15 with powered engines, the CLIP, and test article, and is referred to as the Full Configuration (FC) grid. This FC grid, shown in Figure 7, was the largest with approximately 110.4 million cells and included extra grid refinement on the test article leading edge to capture key flow features for crossflow attenuation in that region.

Rapid aerodynamic design of the test article was not feasible with the FC grid due to its size and complexity, so two smaller grids were created for use in the design process. The first simplified grid was generated with only the CATNLF test article, referred to as the Isolated Test Article (ITA) grid, with coarser surface refinement and is shown in Figure 8. The coarsely refined ITA grid was approximately 4.1 million cells, over 25 times smaller than the FC grid, which enabled efficient evaluation, exploration, and development of the design tools. The simplicity of the ITA grid inherently meant any aerodynamic influence of the F-15 and CLIP on the test article was not captured. Initial flow solutions comparing the ITA and the FC results showed the influence of the F-15 and CLIP imposes a local Mach and angle of attack shift on the test article. The Mach and angle of attack shifts, as described in the equations below, were used during the design development process on the ITA grid. The fin-like orientation of the test article when mounted on the F-15 (seen in Figure 7) means that an aircraft sideslip angle in the FC grid (β_{FC}) equates to a test article angle of attack in the ITA grid (α_{ITA}).

$$M_{ITA} = M_{FC} + 0.02 \quad \text{(Eqn. 1)}$$

$$\alpha_{ITA} = \beta_{FC} + 2 \text{ deg} \quad \text{(Eqn. 2)}$$

The ITA grid was used primarily in the initial design process to develop tools and do the preliminary reshaping needed to obtain laminar flow. While the ITA grid was valuable for initial development, it was necessary to more accurately model the interference effects from the full configuration in the flow solution when designing the final test article shape. Another simplified grid was created to accomplish this goal, referred to as the Full Configuration Design Box (FCDB) grid. The FCDB grid was created using a tool that extracts a portion of an existing unstructured grid and flow solution that is contained within a user-defined box. The flow conditions on the outer faces of this new grid are held constant as boundary conditions, thus maintaining the general influence of the rest of the aircraft in this region while allowing local design changes on the component of interest. This approach significantly reduces the grid size for a more efficient design process, while maintaining grid resolution in the area of interest and accounting for interference effects. For this application, the outer boundary of the FCDB grid was set to approximately 1 test article chord length in every direction from the test article, except for in the direction of the mounting surface where the outer boundary only extended to the surface of the CLIP. The FCDB grid, shown in Figure 9, was approximately 44.3 million cells (approximately 2.5 times smaller than FC) and was used for determining the final design shape of the CATNLF test article. Upon completion of the design, the new test article shape was imported from the FCDB grid into the FC grid. This enabled direct comparison of the FC and FCDB solutions and proved the design box grid accurately modeled the influence of the aircraft and CLIP.

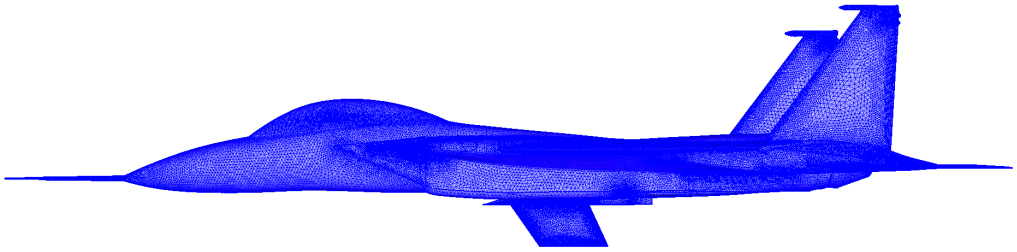

Figure 7. Full Configuration (FC) grid which models the entire flight test configuration, including the fullspan F-15, CLIP, and test article.

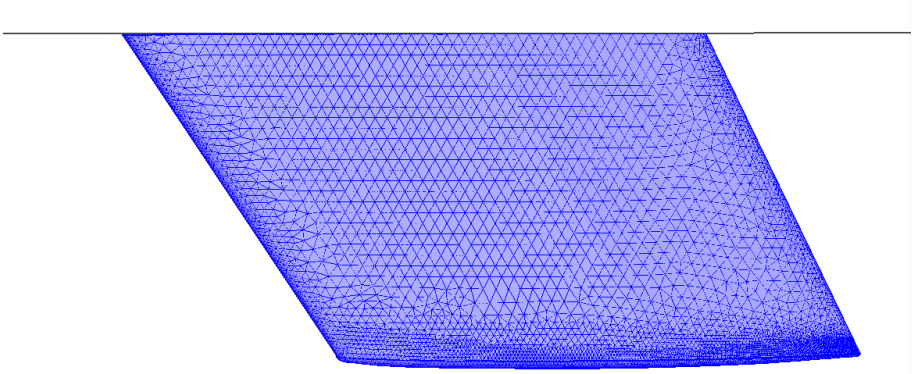

Figure 8. Isolated Test Article (ITA) grid which models only the test article.

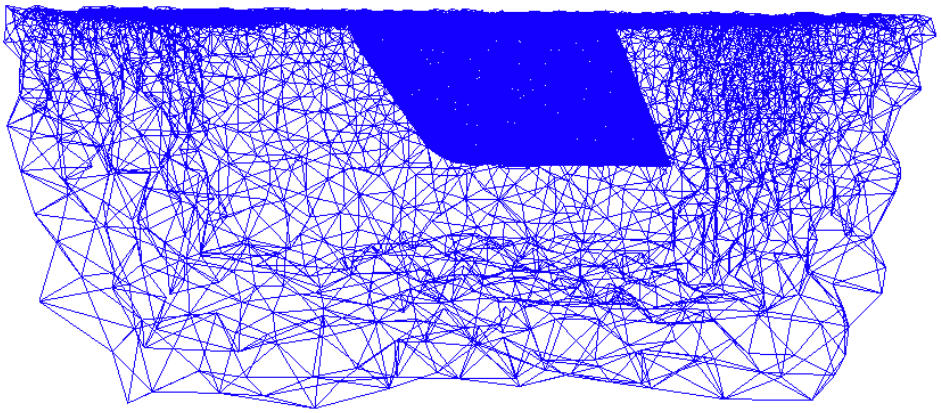

Figure 9. Full Configuration Design Box (FCDB) grid which is extracted from the FC grid to include interference effects from the aircraft and CLIP while reducing grid size for efficient design.

The CATNLF test article was designed using 17 design stations, as shown in the planform view in Figure 10 as black chordwise lines. The three highlighted stations or rows in red, labeled as A, B, and C, are where the static pressure instrumentation will be located on the model. Additional information on the planned instrumentation is discussed in the following section, Testing Strategy for the Flight Test Article. Stations A, B, and C will be used in this paper as example stations to explain the test article design. Table 2 lists some relevant design parameters of these three stations.

The baseline geometry of the test article was generated using NASA SC(2)-0410 supercritical airfoils as a starting point for the design process. The baseline test article showed strong shocks emanating from the leading edge of the root and tip, which significantly decreased the amount of span that could be designed for large extents of laminar flow. To alleviate these shocks, the leading-edge planform of the inboard 10 inches and outboard 5 inches were rounded as illustrated in Figure 10. This altered the root and tip chord lengths from the baseline dimensions shown in Figure 6 to 73.4 and 60.9 inches, respectively. The inboard reduction of leading-edge sweep also helps address attachment line contamination by reducing the Reynolds number based on attachment line momentum thickness (Re_θ) low enough to relaminarize the turbulent attachment line. This method of reducing leading-edge sweep to address attachment line contamination was successfully demonstrated on the previous CRM-NLF wind tunnel model [8, 9]. An assessment of the attachment line transition of the designed test article is provided in the following subsection.

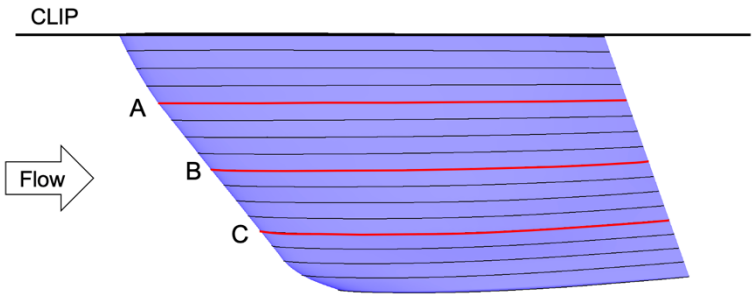

Figure 10. Planform view of the test article showing the 17 design stations, the 3 stations (red) used as examples in this paper, and the planform shape changes of rounding the inboard and outboard leading edge.

Table 2. Relevant parameters of the three example chordwise design stations.

Row	Span Distance from Root	η	Chord	Leading-Edge Sweep	Re_c
A	9.8 in	24%	73.1 in	32.6 deg	32.0 million
B	19.8 in	49%	70.7 in	35.0 deg	30.9 million
C	29.8 in	74%	68.3 in	35.0 deg	29.9 million

The primary objective of this flight test effort is to experimentally validate the CATNLF transition delay method in a flight environment. The transition delay method, as described in the previous subsection, utilizes pressure distributions to suppress the leading-edge CF growth to a subcritical level and grow TS gradually, such that it reaches the designated critical N-factor at a specified transition location. On a standard transonic transport, it would likely be desirable to extend the region of laminar flow as far aft as possible, typically to just ahead of the shock, in order to maximize the drag reduction benefits of laminar flow technology. However, for the research objectives of this flight test effort, it is advantageous to observe a transition front that is not shock limited, i.e., transitions due to TS reaching a critical N-factor rather than transitioning due to a strong pressure gradient or shock. A non-shock-limited TS transition front is expected to move aft as the flight Reynolds number is reduced due to the smaller N-factor growth rate that occurs at lower Reynolds numbers. However, if transition is caused by a shock at the highest Reynolds number, reducing the Reynolds number during flight testing would show little or no difference in the transition location. A design strategy was derived in an attempt to balance the objectives of maximizing the extents of laminar flow, while also characterizing both CF and TS transition in a flight environment. This design strategy aims to have the inboard region of test article maintain laminar flow as far aft as possible, while the outboard region of the test article gradually moves TS transition closer to the leading edge at the design Reynolds number. The inboard portion with an aft transition location will allow for high transition Reynolds numbers to be observed on the test article. The outboard portion with a more forward transition location will enable characterization of Reynolds number effects on laminar flow extents, as well as allow determining the TS critical N-factor experienced in the flight environment. Transition fronts from the target pressure distributions using this design strategy are shown in Figure 11, illustrating the desired progression of the transition location with decreasing Reynolds number.

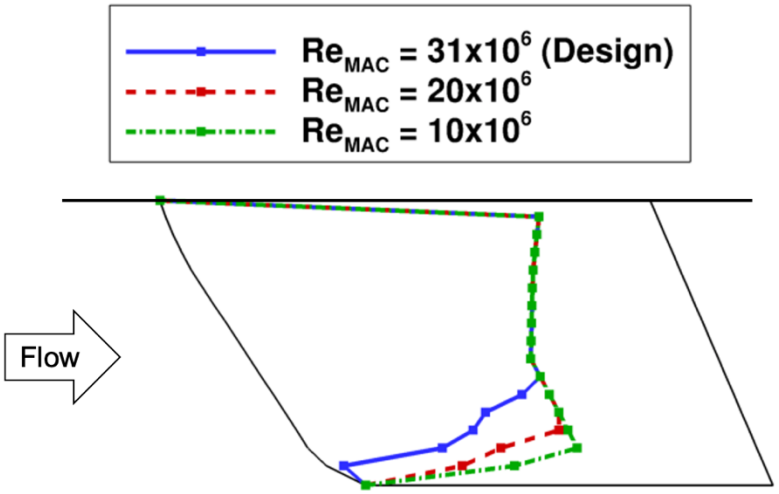

Figure 11. Planform view of the test article with target transition fronts at different Reynolds numbers illustrating the transition design strategy where the inboard portion is shock-limited and outboard is TS transition.

B. Design Results

The aerodynamic design of the CATNLF flight test article has been successfully finalized and is presented in this subsection. While the design was primarily performed on the FCDB grid to save computational resources, all solutions in this section are from the FC grid to fully model the in-flight test environment. The results in the subsection will focus on the design condition of $M_{F\text{-}15} = 0.85$, altitude = 5,000 ft, $Re_{MAC,TA} = 31$ million, $\alpha_{F\text{-}15} = 0$ deg, and $\beta_{F\text{-}15} = 0$ deg. Relevant off-design conditions will be presented in the following subsection.

Figure 12 shows the final design analysis pressures of the test article at Rows A, B, and C. The target pressure distribution is also shown, which is the CATNLF pressure distribution that CDISC is using to drive the airfoil shape changes. The close match between the design and target pressures suggests that the shape changes incorporated by CDISC were effective at obtaining the desired CATNLF pressure architecture. The rapid acceleration at the leading edge was successfully obtained across the span of the test article. The suction-side pressures maintain a relatively constant pressure gradient from the end of the rapid acceleration to just ahead of the shock. This pressure gradient is altered from Row A to C, showing a slightly favorable gradient inboard and a slightly adverse gradient outboard. This change in pressure gradient is needed to obtain the targeted transition characteristics discussed in the previous subsection, where the outboard portion grows TS more rapidly to cause transition ahead of the shock. The small discrepancy in shock location between the design and target pressure distributions at Rows A and B is primarily due to curvature and smoothing geometry constraints on the design airfoils. Overall, the design and target pressures across the span match very well over the entire region where laminar flow is desired, i.e., suction side forward of the target shock. The airfoil shapes needed to obtain these CATNLF pressure distributions are shown in Figure 13. In general, the airfoils resemble typical transport supercritical airfoils. The airfoils have a maximum thickness-to-chord ratio of 10% and have a leading-edge radius nondimensionalized by the local chord of approximately 0.003 across the span. This smaller leading-edge radius is needed to obtain the rapid acceleration of the pressures at the leading edge, as well as reduce the attachment line Re_θ to maintain a laminar attachment line across the span. The test article has a smooth twist distribution with an angle change of approximately 1 deg from 8.57 deg at the root to 7.45 deg at the tip. The test article is mounted to the CLIP at a sideslip angle of -8.57 deg, which imparts a test article angle of attack of +8.57 deg when the aircraft is flying straight and level. This mounting angle allows the test article to obtain the design loading without requiring the pilot to fly at significant sideslip angles during data acquisition. The design maintained the desired sectional loading across the inboard half of the span ($c_l = 0.50$ from $0 < \eta < 0.60$). The outboard portion of the wing smoothly reduced the sectional loading to $c_l = 0.44$ near the wingtip.

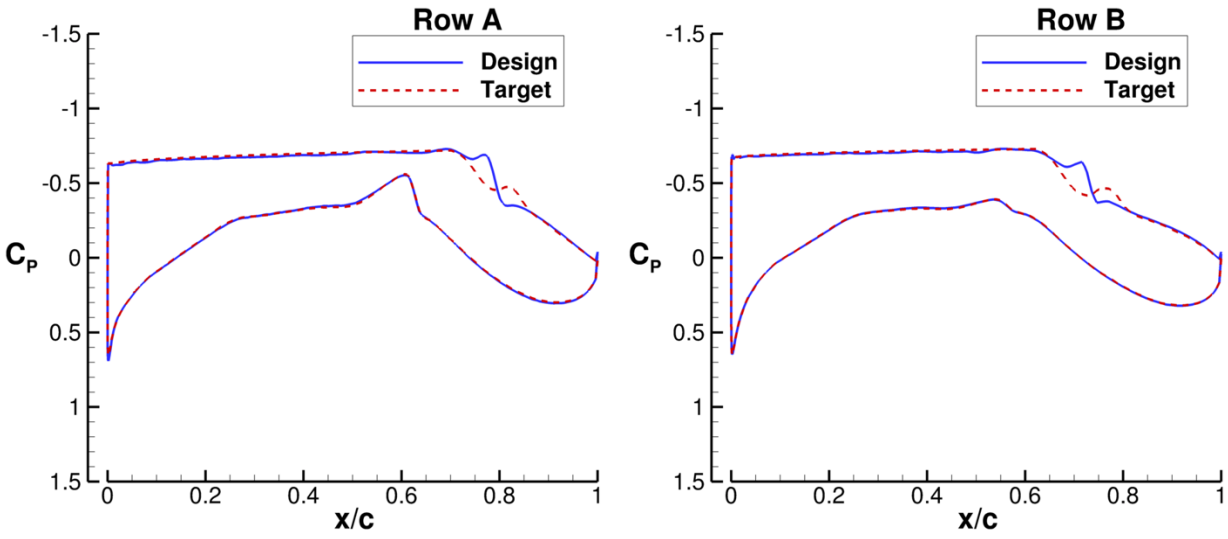

a. Row A

b. Row B

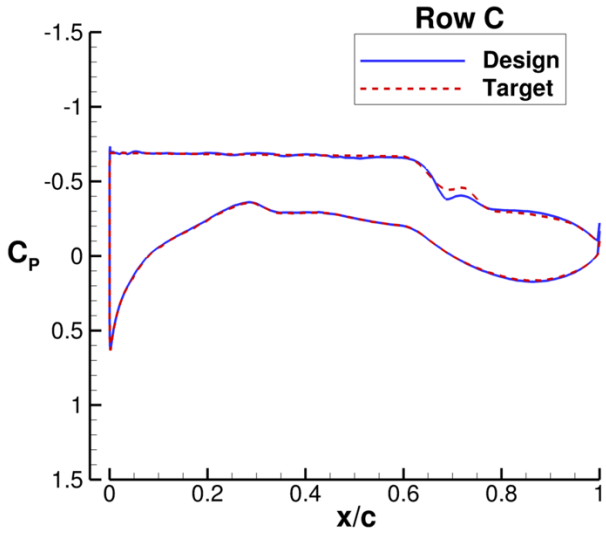

c. Row C

Figure 12. Pressure distributions from the design (blue) test article shape with the target (red) CDISC pressures.

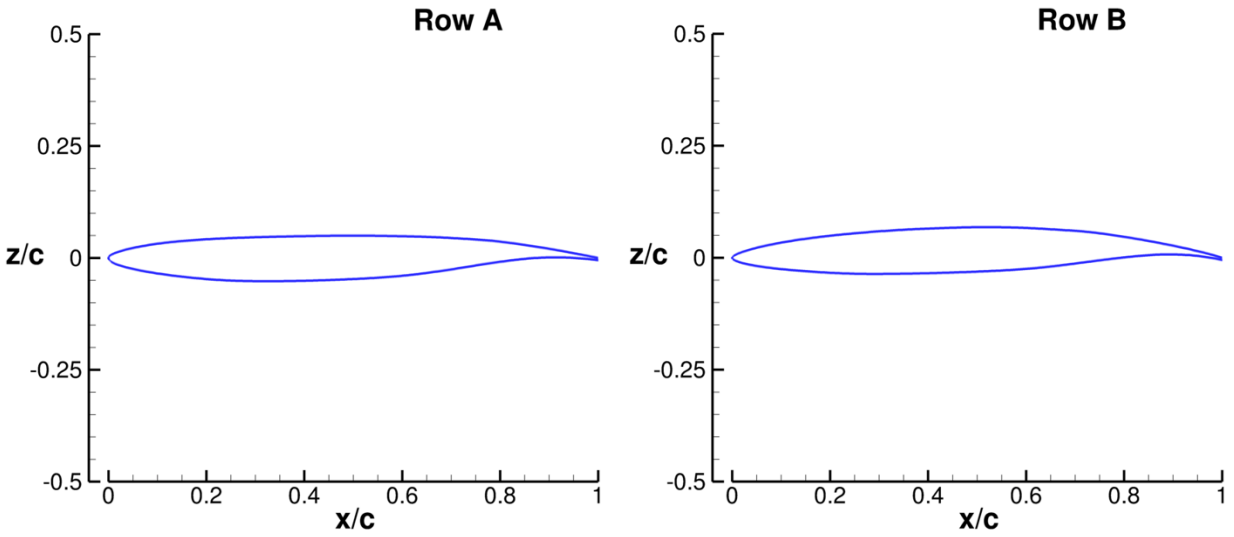

a. Row A

b. Row B

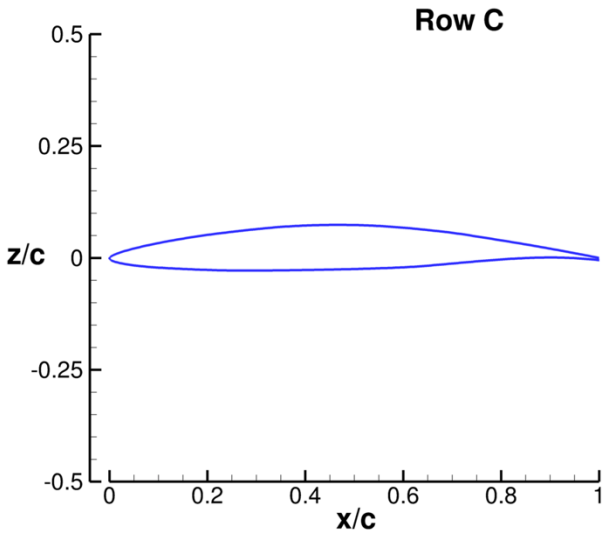

c. Row C

Figure 13. Airfoil shapes nondimensionalized by local chord from the designed test article.

The N-factor growth that corresponds to the design (blue) and target (red) pressure distributions are shown in Figure 14. Both the TS (solid) and CF (dashed) instability growths at each pressure row are plotted. As previously mentioned, this design effort assumed a critical N-factor of 10 for both TS and CF. The figure illustrates good agreement between the design (blue) and target (red) TS and CF growth, which is further confirmation that CDISC was successful at driving the design to the desired laminar flow characteristics. The CF character of rapid growth very near the leading edge is typical for lifting components with high sweep and high Reynolds number. The CATNLF pressure architecture has successfully controlled the CF growth such that it remains subcritical near the leading edge and quickly damps out after the initial rapid growth. All 3 pressure rows demonstrate lower leading-edge maximum CF values for the design compared to the target pressures. This is likely due to a very small leading-edge pressure spike found on the design pressures that further damps the CF in that region. The maximum CF N-factor at the leading edge reduces from root to tip due to the reduction in chord Reynolds number out the span. Both the design and target TS N-factors grow gradually from the leading edge as desired. The TS calculations terminate slightly forward of the shock. As neither Row A nor B reach the designated critical N-factor of 10 before terminating, it is assumed these spanwise locations will have shock-limited extents of laminar flow at an x/c of 0.70 for Row A and 0.62 for Row B. The design at Row C reaches an N-factor of 10 at an x/c of 0.37, suggesting this region of the test article will transition

due to TS forward of the shock at the design condition. The predicted transition Reynolds numbers (i.e., Reynolds number based on the chordwise extent of laminar flow) for Rows A, B, and C are 22.4, 19.2, and 11.0 million, respectively.

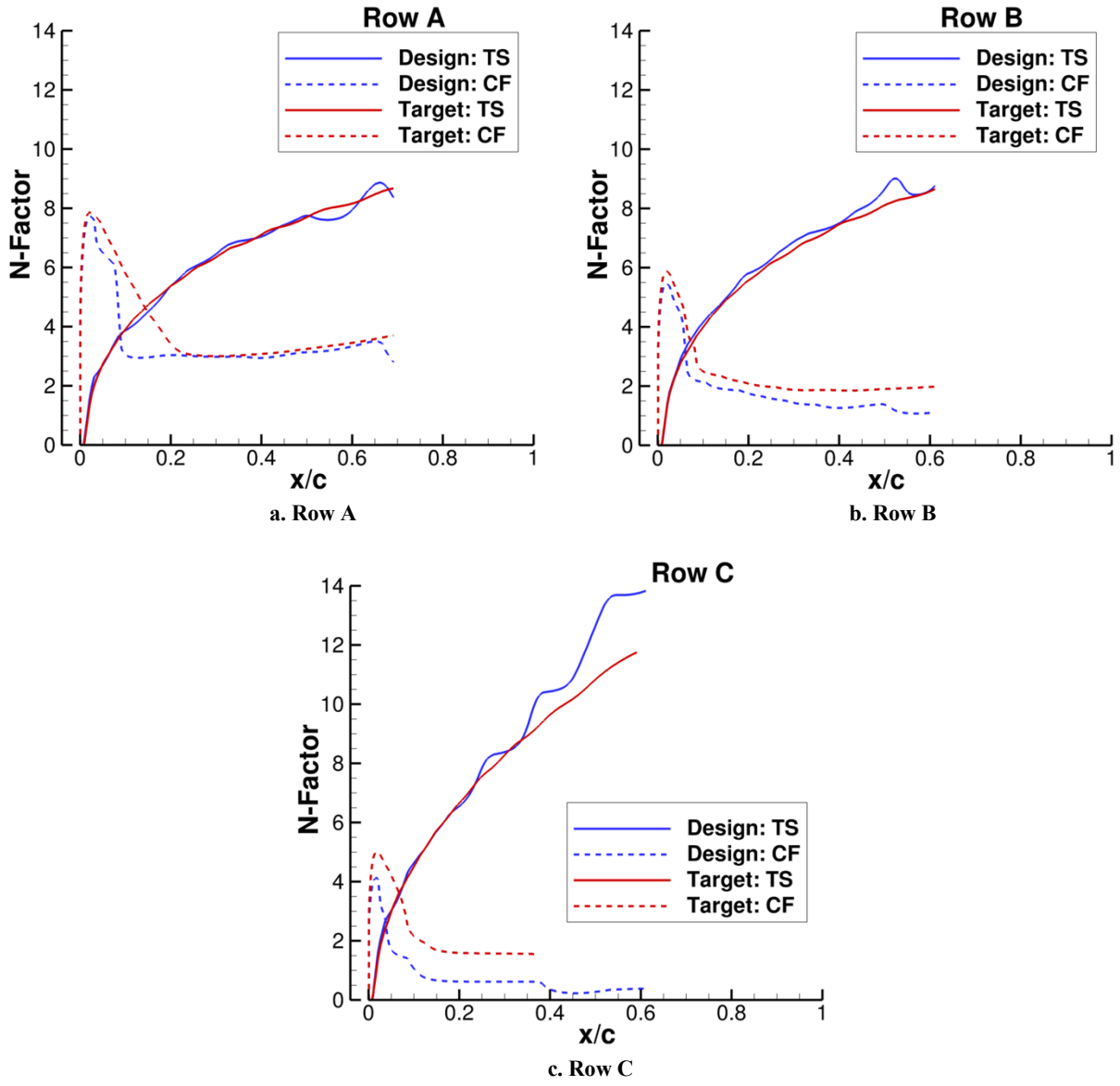

a. Row A

b. Row B

c. Row C

Figure 14. N-factor growth from the design (blue) and target (red) pressure distributions for both TS (solid) and CF (dashed).

In addition to the TS and CF instabilities, the design addresses transition due to a turbulent attachment line. For this analysis, the attachment line Re_θ value is calculated via the BLSTA3D code at each spanwise station. The spanwise distribution of the attachment line Re_θ is shown in Figure 15. As discussed previously, the reduced sweep section inboard helps to reduce the attachment line Re_θ below Poll's criteria of 100, which should relaminarize the attachment line contamination that occurs from the turbulent boundary layer on the CLIP running onto the swept test article [19]. Outboard of this short relaminarization region, the test article must stay below Poll's criteria of 235 for attachment line transition. The figure shows this transition criteria is met across the span of the test article, suggesting that attachment line transition should be avoided successfully on the test article at the design condition. The test article will be susceptible to attachment line bypass transition, where the attachment line is tripped due to a surface imperfection at the attachment line, because the Re_θ values are above 100 for the majority of the span. This type of

transition was observed and analyzed in the wind tunnel test of the CRM-NLF model [8, 9]. The unit Reynolds number required to obtain the design mean aerodynamic chord Reynolds number for the flight test is reduced compared to the previous CRM-NLF NTF wind tunnel test due to the increased model size in flight. These reduced unit Reynolds numbers, as well as implementing testing strategies that aim to keep the leading edge clear of surface imperfections, are expected to help alleviate this attachment line bypass transition. Additionally, a reduction in flight Reynolds number will provide further protection against attachment line bypass transition because the attachment line Re_θ values will decrease with flight Reynolds number.

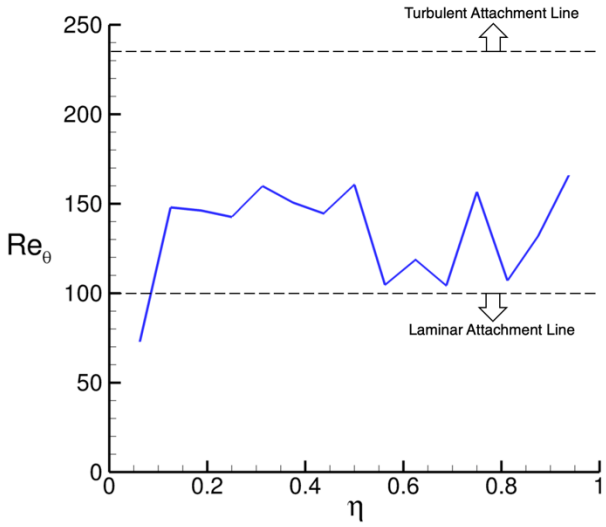

Figure 15. Spanwise distribution of the attachment line Re_θ values for the test article design with Poll's criteria for attachment line state.

The laminar flow extents of the test article are illustrated in the transition front image shown in Figure 16. This figure compares the design and target transition locations across the span. The agreement between the two fronts provides further evidence of the success of the CDISC design method to meet the desired design characteristics. The final design of the test article is predicted to support laminar flow on approximately 53% of the surface area on the suction side. The largest predicted transition Reynolds number was 25.7 million at an inboard station on the reduced-sweep section (23 deg leading-edge sweep) where the design shock was further aft of the targets at an x/c of 0.80. While this transition Reynolds number would still be higher than historic NLF data, the reduced leading-edge sweep at that location moves the point away from the zone of relevant modern twin-aisle transonic transport wings based on sweep. The highest predicted transition Reynolds number on the constant 35 deg leading-edge sweep section of the test article was 21.6 million, located just outboard of Row A. Figure 17 compares this predicted maximum transition Reynolds number to previous NLF experiments at transonic transport relevant sweeps (noted by the gray band of sweeps) on the laminar flow extent versus wing sweep plot from Figure 1. The CATNLF flight test symbol is open to signify the data point is a computational prediction, whereas the other data on the plot are experimentally validated. This predicted maximum transition Reynolds number represents over three times more laminar flow than the previous maximum seen in experimental data on configurations with comparable wing sweeps not using the CATNLF method. The relatively high computational transition predictions of the test article suggest the CATNLF design method would significantly expand the NLF potential to modern transonic transport wings.

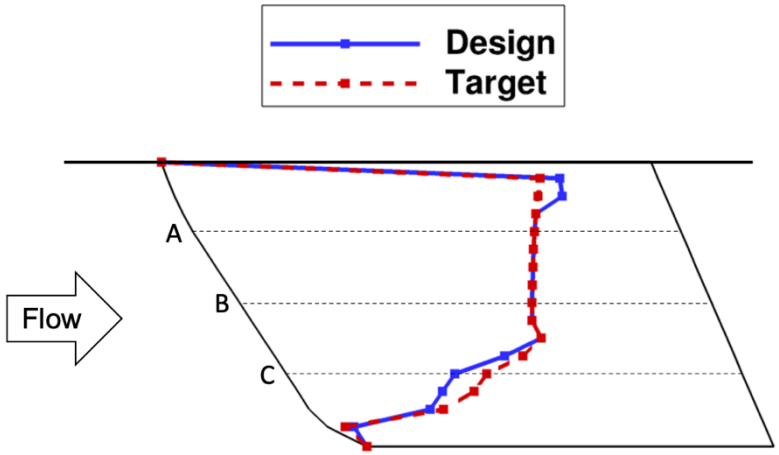

Figure 16. Planform view of the suction-side showing the predicted transition fronts for the design (blue) and target (red) pressures.

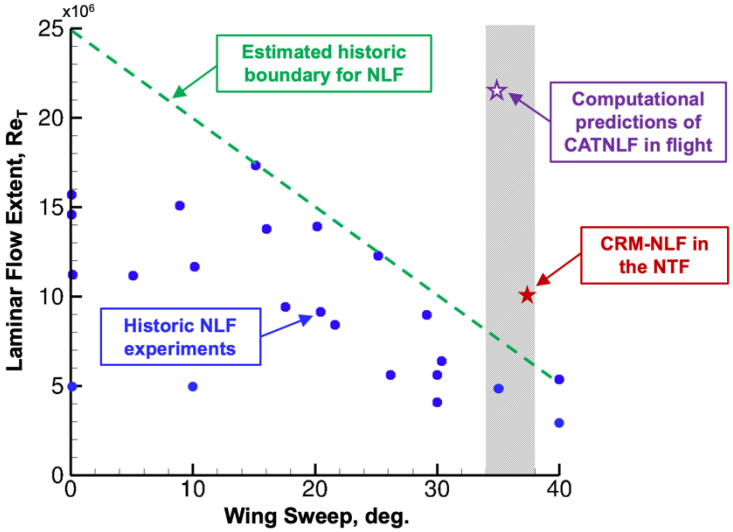

Figure 17. Laminar flow extent versus wing sweep plot from Figure 1 including predictions for the CATNLF test article.

C. Off-Design Results

In an effort to gather flight data that will further the understanding of laminar flow wings, it is desirable to test off-design conditions that may illustrate trends or characteristics of the CATNLF flight test article. These off-design conditions include variations in test article Reynolds number, obtained by changing altitude, and test article angle of attack, obtained by changing aircraft sideslip angle. The aim of these off-design conditions is that the data may be used to quantify a flight-environment critical N-factor value, as well as confirm that the CATNLF design method is robust enough to support laminar flow at off-design conditions. This subsection will present the computational predictions for these off-design conditions. Additional off-design conditions are considered in order to evaluate the potential impact of flight condition variability during data acquisition, including small perturbations in Mach number and aircraft angle of attack (test article sideslip).

As mentioned previously, the CATNLF test article was designed to support significant extents of laminar flow at a mean aerodynamic chord Reynolds number of 31 million. The design strategy, illustrated in Figure 11, was to have the inboard portion of the wing support a large chordwise extent of laminar flow that was limited by the shock, and the outboard portion of the wing transitioning due to TS forward of the shock at the design Reynolds number. Reducing

the Reynolds number during data acquisition would suppress the TS and move the outboard transition front further aft. An example of the impact of reducing Reynolds number on the pressure distributions at the midspan station of Row B is found in Figure 18. The plot shows that Reynolds number has negligible impact on the pressure distribution, with the only notable differences being the forward progression of the shock location and very slight reduction in aft loading with reduced Reynolds number. While the changes in pressure distributions with Reynolds number are minimal, Figure 19 shows the significant reduction in N-factor growth that occurs at reduced Reynolds number conditions. Both the TS (solid) and CF (dashed) instabilities maintain similar growth features across the Reynolds number range due to the mostly unaltered pressure distributions, but the overall level of N-factor values is significantly reduced with Reynolds number. The maximum N-factor reached is reduced by approximately 4 for both TS and CF from the 31 million to the 10 million Re_{MAC} condition. The reduction in N-factor value at Row B is not expected to increase the extent of laminar flow because the critical N-factor of 10 is not reached before the shock at the highest Reynolds number at this spanwise location. The impact of reducing Reynolds number on the transition front is shown in Figure 20. In general, the inboard portion of the wing that has shock-limited extents of laminar flow is unchanged. The pressure distribution in Figure 18 showed forward movement of the shock with reduced Reynolds number, which could move the transition front forward for lower Reynolds numbers, as seen over a small region inboard where the Reynolds number of 10 million front (green) is further forward. However, over the majority of the inboard section, the boundary layer instability calculations used for these predictions all terminate slightly ahead of the shock where the pressures begin an adverse gradient (an example is shown on Row B at x/c = 0.63). This early termination of the boundary layer instability calculations causes the majority of the shock-limited portion of the front to be unchanged regardless of the slight shock movement that occurs with Reynolds number reduction. The outboard region of the test article shows transition front variation with Reynolds number. Row C shows an aft progression of the chordwise transition location of x/c = 0.37, 0.49, and 0.60 at Re_{MAC} of 31, 20, and 10 million, respectively. This chordwise transition location is shifting because of the reduction in N-factor values, like those seen in Figure 19, causing the critical N-factor to be reached further aft on the airfoil. Because this outboard region is transitioning when the critical N-factor is reached, rather than when the laminar boundary layer encounters a shock, the intention is to use this set of Reynolds number data to quantify the critical N-factor in the flight environment under the F-15 aircraft.

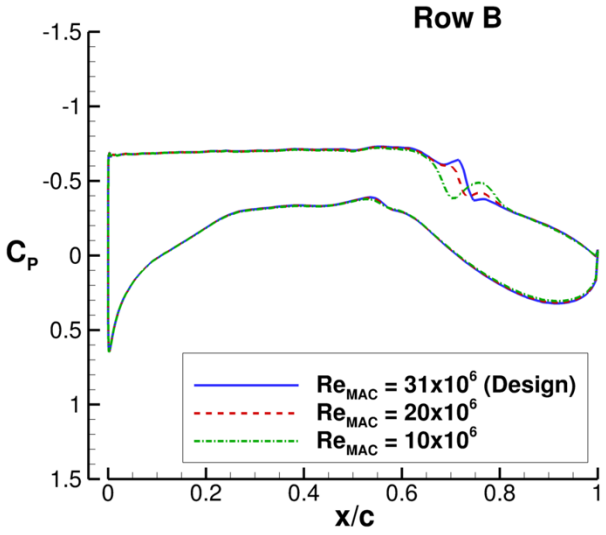

Figure 18. Pressure distributions at Row B for a variety of Reynolds numbers.

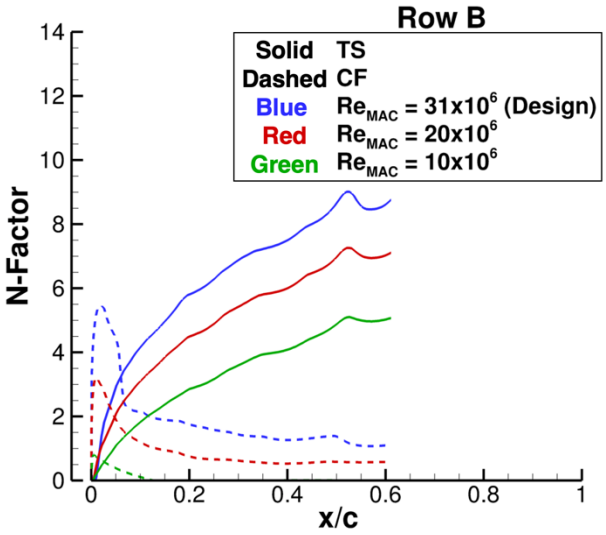

Figure 19. N-factor growth for TS (solid) and CF (dashed) at Row B for a variety of Reynolds numbers.

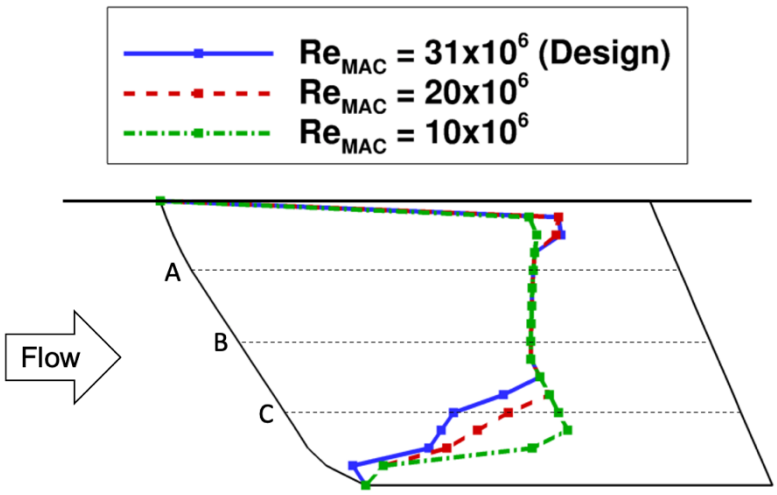

Figure 20. Planform view showing the predicted transition fronts for a variety of Reynolds numbers.

Another significant off-design condition used to characterize the CATNLF test article is the aircraft sideslip angle ($\beta_{F\text{-}15}$), which causes different loadings on the test article by altering the test article angle of attack. For a practical wing design method, it is desirable to maintain the drag-saving benefits of laminar flow at near-cruise conditions. For the CATNLF test article, an aircraft sideslip angle of -1 deg creates a +1 deg angle of attack change, which results in approximately +10% design sectional lift coefficient change ($c_l = 0.55$). Similarly, an aircraft sideslip angle of +1 deg creates a -1 deg test article angle of attack change that produces approximately -10% design sectional lift coefficient change ($c_l = 0.45$). The impact on the pressure distribution at Row B with changing aircraft sideslip angle is shown in Figure 21. As the loading on the test article is increased (red, $\beta_{F\text{-}15} = -1$ deg), the flow is accelerated more at the leading edge creating a pressure spike, and the suction-side pressures encounter a more adverse pressure gradient to the shock. Conversely, as the loading on the test article is decreased (green, $\beta_{F\text{-}15} = +1$ deg), the flow is accelerated less than the design condition at the leading edge with a much more rounded leading edge pressure distribution, after which the suction-side pressures encounter a more favorable pressure distribution. The changes in these pressure distributions create differences in both the TS and CF N-factor growth, seen in Figure 22. The TS growth character is altered by the discussed changes in the midchord, suction-side pressure gradients, where the adverse gradient seen on the higher-loaded test article (red, $\beta_{F\text{-}15} = -1$ deg) causes growth in TS values and the favorable gradient seen on the lower-loaded test article (green, $\beta_{F\text{-}15} = +1$ deg) causes reduction in TS values compared to the design condition (blue). The leading-edge CF values are mostly unchanged, with slight maximum N-factor value changes corresponding to the delta C_P occurring in the initial flow acceleration at the different sideslip conditions. The most notable change in CF character with test article loading occurs in the midchord region, where the lower-loaded condition (green, $\beta_{F\text{-}15} = +1$ deg) has regrowth of CF after the initial leading-edge growth. This regrowth in CF occurs due to the favorable pressure gradient at this condition. The regrowth of CF is not expected to reach the critical N-factor of 10 prior to the shock, so no impact on the transition locations is expected due to the changes in CF. The transition front comparing the three test article loading conditions is found in Figure 23. The impact of the increase in TS growth at the higher-loaded condition (red, $\beta_{F\text{-}15} = -1$ deg) is seen by a loss in laminar flow extent compared to the design condition (blue). There is a slight increase in laminar flow extent predicted at the lower-loaded condition. The predicted surface areas of laminar flow on the suction side of the test article are 53%, 37%, and 55% for the $\beta_{F\text{-}15} = 0$ deg (design), $\beta_{F\text{-}15} = -1$ deg, and $\beta_{F\text{-}15} = +1$ deg conditions, respectively.

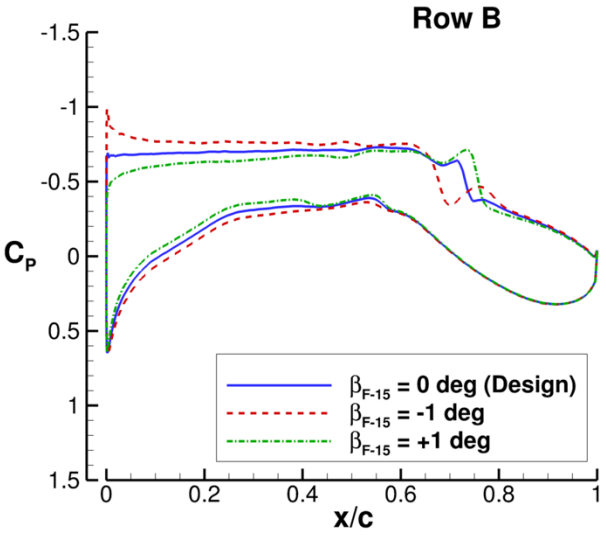

Figure 21. Pressure distributions at Row B for a variety of aircraft sideslip angles that produce a test article angle of attack change.

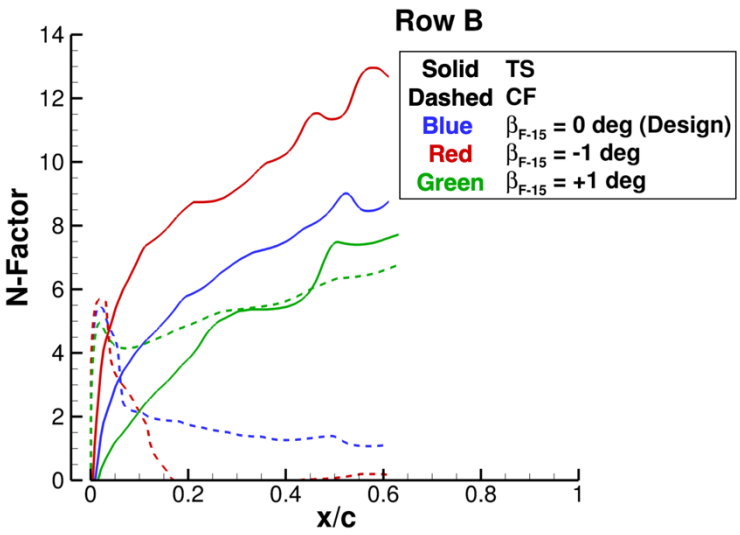

Figure 22. N-factor growth for TS (solid) and CF (dashed) at Row B for a variety of aircraft sideslip angles that produce a test article angle of attack change.

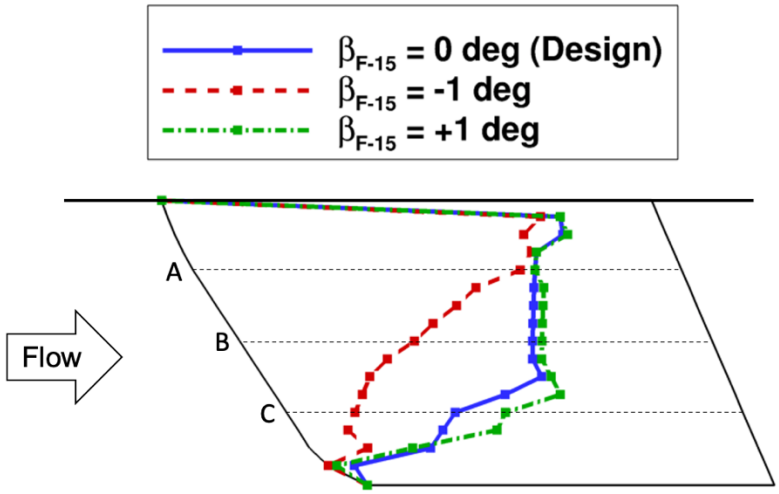

Figure 23. Planform view showing the predicted transition fronts for a variety of aircraft sideslip angles that produce a test article angle of attack change.

Small variations in aircraft Mach and angle of attack are also considered to evaluate the impact of potential flight condition variations during data acquisition. For this study, perturbations of +/- 0.01 in M_{F-15} and +/- 1 deg in α_{F-15} are considered. Due to the vertical mounting of the test article underneath the F-15, a positive F-15 angle of attack change creates a sideslip angle on the test article, effectively a reduction of sweep on the test article. Figure 24 shows the pressure distributions at Row B for both the M_{F-15} and α_{F-15} ranges considered. A notable similarity in pressure distributions occurs between the M_{F-15} = 0.84 and α_{F-15} = +1 deg conditions and between the M_{F-15} = 0.86 and α_{F-15} = -1 deg conditions. This similarity can be explained when considering the normal Mach number, analogous to that calculated in simple sweep theory, which would suggest a change in sweep of 1 deg would create a change in normal Mach number of approximately 0.01. The reduction in Mach number (M_{F-15} = 0.84) and reduction of sweep (α_{F-15} = +1 deg) show a more forward shock and a slightly adverse pressure gradient. Conversely, the increased Mach number and sweep conditions (M_{F-15} = 0.86 and α_{F-15} = -1 deg) show a stronger, further aft shock and a slightly favorable pressure gradient. The impact of these pressure changes on the TS and CF N-factor growth is shown in Figure 25. The TS values respond to the slight changes in pressure gradients as expected, but the most notable change is that the

$M_{F\text{-}15}$ = 0.84 and $\alpha_{F\text{-}15}$ = +1 deg solutions terminate prematurely at approximately x/c = 0.40. This early termination can be correlated to the sharp adverse pressure gradient seen at x/c = 0.40 for these solutions, which causes the laminar boundary layer to terminate in the boundary layer profile solver, BLSTA3D. The early termination of the solution is where the presumed transition location would occur. The CF values for both the Mach and aircraft angle of attack sweeps are relatively unchanged and show only small variations in the regrowth of CF after the initial leading-edge growth due to the slight changes in pressure gradients. The predicted transition fronts for the Mach and aircraft angle of attack conditions are shown in Figure 26. These fronts show a greater loss of laminar flow at the lower Mach number ($M_{F\text{-}15}$ = 0.84) and lower test article sweep ($\alpha_{F\text{-}15}$ = +1 deg) conditions.

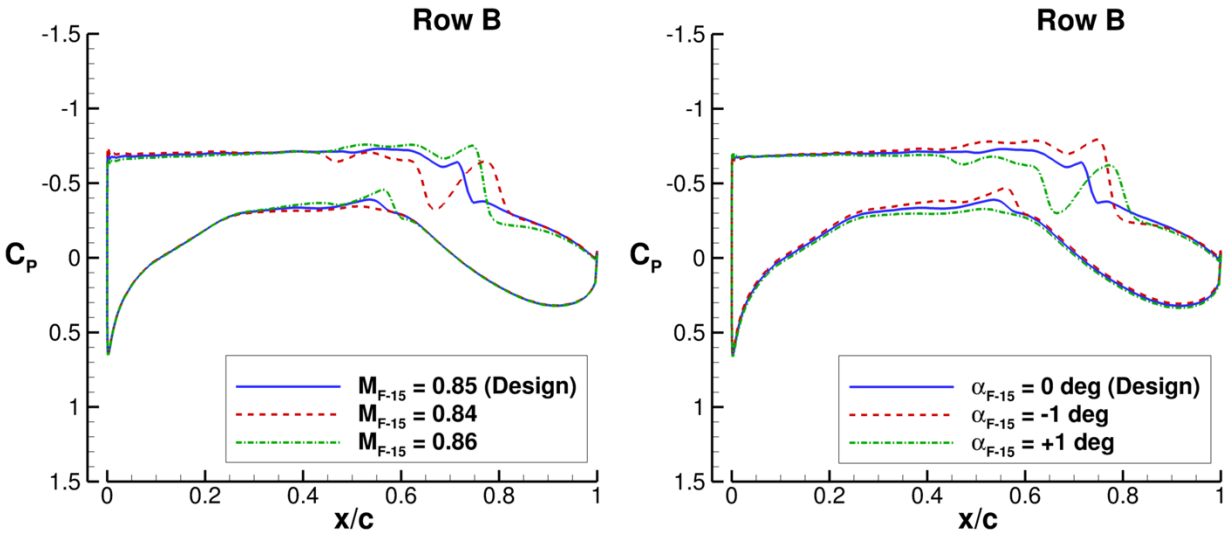

a. Mach **b. Aircraft angle of attack**

Figure 24. Pressure distributions at Row B for a variety of Mach and aircraft angle of attack conditions.

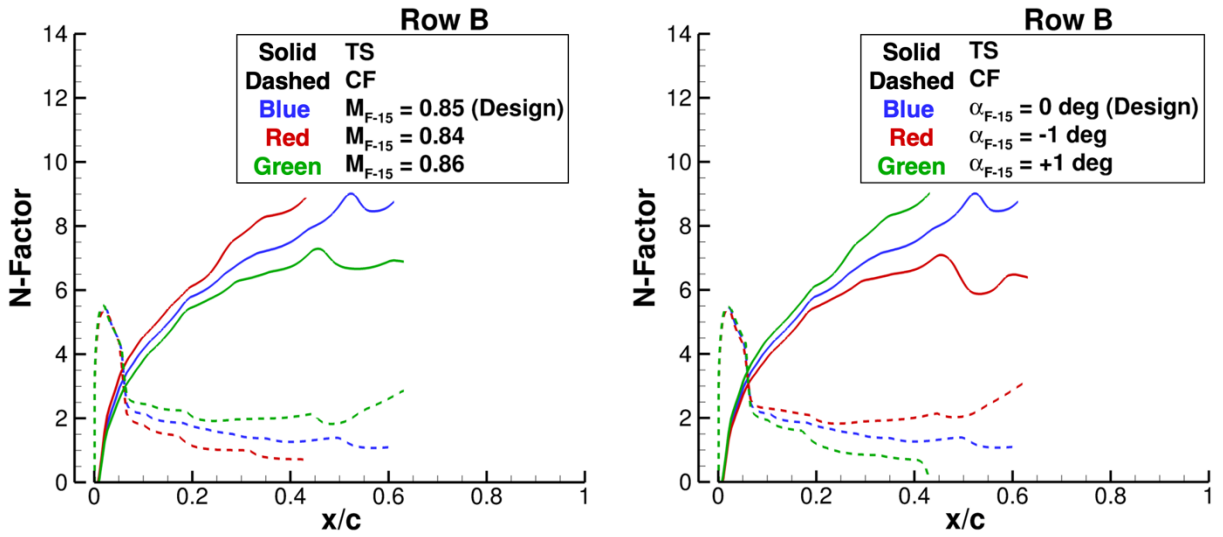

a. Mach **b. Aircraft angle of attack**

Figure 25. N-factor growth for TS (solid) and CF (dashed) at Row B for a variety of Mach and aircraft angle of attack conditions.

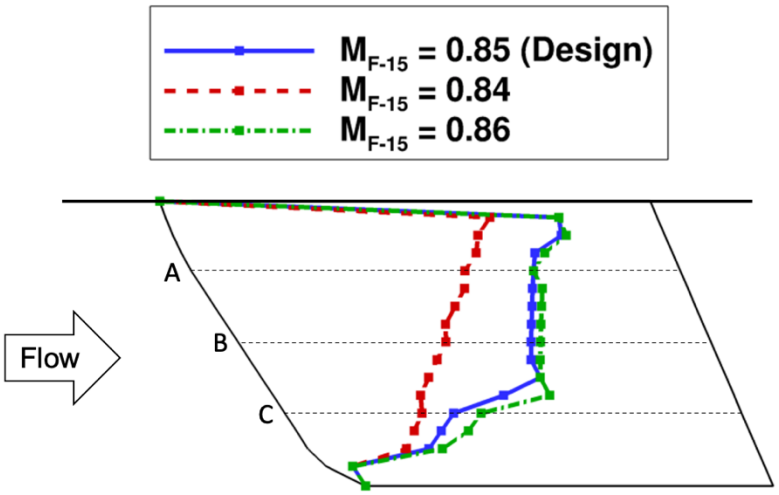

a. Mach

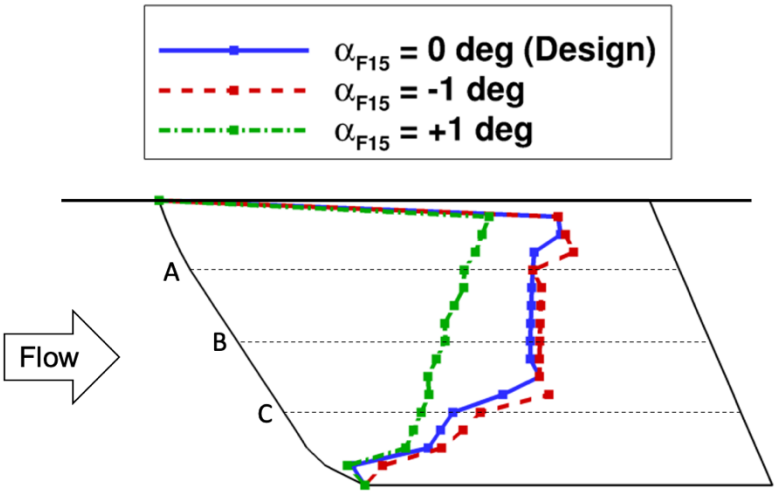

b. Aircraft angle of attack that produces a test article sideslip angle change

Figure 26. Planform view showing the predicted transition fronts for a variety of Mach and aircraft angle of attack conditions.

One important assumption in the design of the CATNLF test article that can impact the predicted extents of laminar flow is the critical N-factor. This critical N-factor value is dependent on several factors, including the freestream turbulence levels and stability analysis method employed when calculating the value. Because the test article is flying underneath an F-15, there is some uncertainty about how the F-15 interference affects the freestream turbulence levels in the vicinity of the test article. A Flow Rake flight test is scheduled before the CATNLF flight test to gather relevant data to characterize the flow environment underneath the F-15. However, those data will not be available until after the test article is manufactured, so it could not be used to determine the critical N-factor needed for the design. As mentioned previously, a critical N-factor of 10 was selected for both TS and CF to represent a flight environment for this design work. All previously shown transition fronts use this assumed critical N-factor of 10 for the computational predictions. Figure 27 shows the impact on the laminar flow extent that can be expected at the design condition with variations of the assumed critical N-factor. An increase in critical N-factor, which represents a better-than-expected turbulence level underneath the F-15, would result in minimal changes to the laminar flow extent inboard because that region of the wing is shock limited. The outboard potion of the wing would expect a small increase in laminar flow

extent if a higher critical N-factor is experienced. A decrease in critical N-factor, which represents higher turbulence levels underneath the F-15 than presently assumed, shows more significant changes to the laminar flow front. For the critical N-factor = 8 front (red), the majority of the wing is transitioning due to TS ahead of the shock. There are two stations inboard that transition due to CF very near the leading edge. If the critical N-factor is reduced further, additional leading-edge CF transition would be expected, beginning inboard where the higher maximum CF N-factors occurred, similar to the example in Figure 14. While the critical N-factor had to be assumed for the design process, Figure 27 shows that variations in both directions on the assumed critical N-factor (10) still show significant extents of laminar flow. The research objectives of the CATNLF test article are presently expected to be successful even if the critical N-factor differs from the assumed value, and hopefully the test can be used to quantify the flight environment critical N-factor with more confidence so future flight tests can use a more calibrated value.

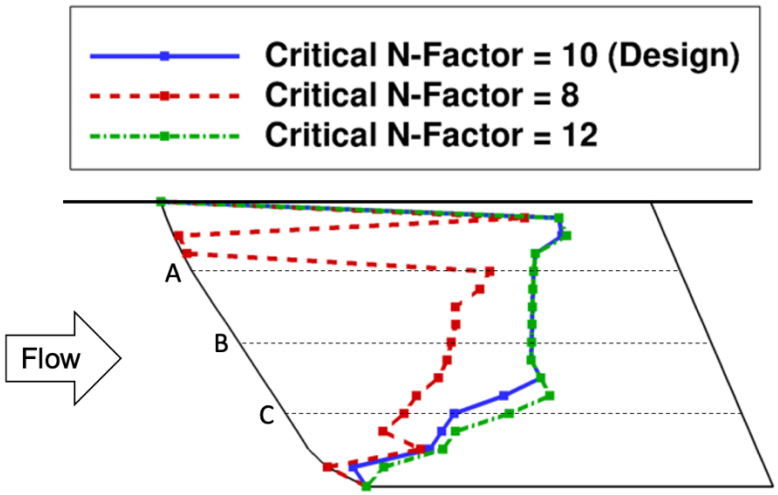

Figure 27. Planform view showing the predicted transition fronts for a variety of critical N-factors.

IV. Testing Strategy for the Flight Test Article

The flight test article has been aerodynamically designed to evaluate the CATNLF transition delay method in a flight environment underneath the F-15 testbed. The flight conditions and data acquired for the experimental investigation have been chosen such that two primary goals can be evaluated. This section will include information on these two primary goals, including the motivation, test conditions, and planned test article instrumentation that will help evaluate these goals.

A. Primary Flight Test Goals

The primary goal of the CATNLF flight test is to confirm the effectiveness of the CATNLF method in attenuating crossflow growth at conditions representative of a modern transonic transport wing. The wing was designed to be as similar to a transonic transport wing as possible given the size constraints the testbed imposed on the test article. As discussed previously, the test article is a lifting surface with supercritical airfoils and has 35 deg leading-edge sweep across the majority of the span. In order to evaluate the crossflow attenuation strategy, the test article will be tested at low altitudes to produce the high unit Reynolds numbers required to obtain the desired high Re_{MAC} on the test article. Crossflow growth is strongly correlated to Reynolds numbers, so the high Re_{MAC} values are needed to better represent the typical crossflow growth on a transonic transport. For this test, the evaluation of the CATNLF transition delay method will be between Re_{MAC} values of 15 and 31 million, as seen in Table 3.

The secondary goal of the CATNLF flight test is to investigate the surface requirements for laminar flow applications on transonic transport wings. Due to the test article size limitations imposed by the testbed, relatively high unit Reynolds numbers (Re') are needed in order to obtain these transport-relevant Re_{MAC}. Since bypass transition and transition related to surface roughness are directly correlated to Re', it was advantageous to establish this secondary goal to investigate surface requirements needed at transport-relevant Re'. For this secondary goal, Re' values ranging from 1.0 to 3.4 million/ft will be tested (shown in Table 3), which covers the Re' range seen on current transport aircraft such as the B737 and B777 during transonic cruise. The method for evaluating surface requirements

is still being finalized, but current proposals include incrementally roughening the surface and/or adding known-height imperfections, and studying the impact on laminar flow extents.

Table 3. Planned flight test conditions for the two primary goals of the CATNLF test article.

Altitude (ft)	5,000*	12,500	19,600	28,500	39,000	49,500
M_{F-15}	0.85 +/- 0.01	0.85	0.85	0.85	0.85	0.85
β_{F-15} (deg)	+/- 1.0	+/- 1.0	+/- 1.0	+/- 1.0	+/- 1.0	+/- 1.0
α_{F-15} (deg)	0.0	0.0	0.0	0.0	0.0	0.0
Re' ($x10^6$/ft)	5.3	4.2	3.4	2.6	1.7	1.0
Re_{MAC} ($x10^6$)	31	25	20	15	10	6
Goal**	1	1	1 / 2	1 / 2	2	2

*Test article design condition

**Goals:

1) Transport-relevant Re_{MAC} for CATNLF evaluation

2) Transport-relevant Re' for surface finish requirements evaluation

Additional flights are proposed to include a DRE study for the CATNLF test article after the first two objectives are met. The details of this study are still being finalized, but would have the goal of using DREs to extend the length of laminar flow similar to the effects seen on the Swept-Wing Laminar Flow (SWLF) flight test [12]. This study would likely focus on off-design conditions that have transition fronts that are not shock-limited.

B. Test Article Instrumentation

The CATNLF test article will be manufactured with several instrumentation capabilities to enable the successful evaluation of the two primary goals and the potential DRE study. The primary source of data for this test is the transition visualization data, which will be acquired via an existing infrared (IR) camera system attached to the F-15 that views the righthand (suction) surface of the test article in flight. To improve the quality of this IR transition visualization data, a carbon-based resistive heating layer will be used to provide the required temperature gradient used to visualize laminar flow. This heating layer was experimentally validated in both the CRM-NLF wind tunnel test and the ReHEAT flight test [13, 20].

The test article will be instrumented with static and dynamic pressure sensors, subsurface thermocouples, internal electrical wires for the resistive heating layer, and wingtip accelerometers to aid in the evaluation of the research goals. The instrumentation layout for the test article is provided in Figure 28. In addition to the aforementioned IR transition visualization data, another key source of data for this flight test is the static pressure data, which will be used to confirm that the CATNLF pressure architecture is obtained on the flight test article. Chordwise static pressure orifices will be manufactured into the model at 3 spanwise stations to acquire this data, located at the previously identified Rows A, B, and C. The static pressure orifices near the leading edge will have a smaller diameter in an attempt to reduce the occurrence of bypass transition caused by the pressure orifices where the boundary layer is smallest. Subsurface thermocouples will be incorporated into the model to provide surface temperature data in chordwise distributions at 3 spanwise stations approximately 1 inch inboard of each static pressure row. Additionally, the test article will have 3 clusters of flush-mounted dynamic pressure sensors for crossflow and unsteady shock data. Two of the dynamic pressure sensor clusters will be arranged in a triangular fashion closer to the leading edge on removable plugs, similar to the arrangement used in the SWLF flight test [12], to acquire the dynamic pressure data that is helpful in characterizing boundary layer instabilities. The remaining dynamic pressure sensors cluster will be arranged in a chordwise fashion to pick up any unsteady shock behavior, such as the one identified on the CRM-NLF model [8]. The resistive heating layer will have the required power source provided via an internal electrical wire that exits the instrumentation cavity to the surface at 4 locations. The resistive heating layer will wrap around the leading edge in order to avoid any steps caused by the paint that may lead to transition. The test article will also be instrumented with 4 accelerometers at the leading and trailing edges of the wingtip in order to monitor any undesirable dynamic stability characteristics during flight.

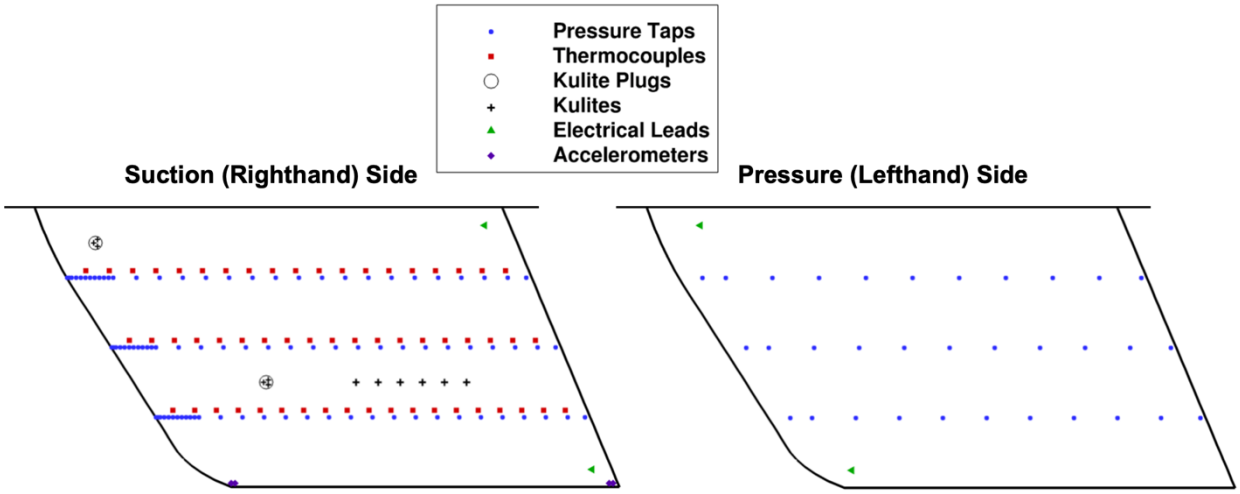

Figure 28. Planform view showing the instrumentation layout on both the suction (left) and pressure (right) side.

The F-15 flight conditions, including Mach number, altitude, angle of attack, and angle of sideslip, will be recorded throughout data acquisition as well. These F-15 flight conditions, along with the pressure distributions from the static pressure ports, will be used to identify the conditions the test article is experiencing. Relevant surface quality data, such as surface roughness measurements, paint thickness measurements, and high-quality photographs, will be collected before and after each flight at specified locations on the test article. If necessary, the test article will be sanded and polished to remove any surface imperfections that occur during testing.

C. Potential Wind Tunnel Testing of Test Article

It has been proposed that the CATNLF test article be tested in a wind tunnel to provide a direct comparison of laminar flow extents in two environments. This would likely take place after the flight test effort in a facility that would support a wide range of test Reynolds numbers, such as the 11- by 11-foot Transonic Wind Tunnel at the NASA Ames Research Center or the NTF at the NASA Langley Research Center. The primary objective of this experiment would be to acquire data that enables direct comparison of laminar flow in two different environments on the same test article, similar to the wind tunnel and flight experiments of the SWLF test article [12].

The CATNLF test article was designed in the presence of the F-15 and CLIP to account for aerodynamic interference on the test article. Differences between the test article pressures from the FC and ITA grids highlighted the significance of this aerodynamic interference. The Mach and angle of attack shifts employed when using the ITA grid accommodated for some interference and was adequate for the initial design and tool development phase of the CATNLF design project. However, these simple Mach and angle of attack shifts are not adequate to fully account for the complexity of the F-15 flow field. In the wind tunnel, the F-15 would not be present, which eliminates the ability to isolate the effects of environment on the laminar flow extent rather than the effects of the missing aerodynamic interference. One possible solution is to design and manufacture a wind-tunnel-compatible surface that provides equivalent loading on the test article. An initial investigation into this surface design concept has been performed with promising results, confirming the viability that a generic surface, similar to a wind tunnel liner, could produce test article pressures that match those predicted when mounted on the F-15 aircraft. This equivalent surface could enable direct comparison of the laminar flow extent in both a wind tunnel and flight environment on the CATNLF test article. Additionally, it would allow the CATNLF test article geometry and experimental data to be released with a publicly-releasable interference surface for use in computational studies.

V. Concluding Remarks

The CATNLF boundary layer transition delay method was developed to provide significant drag reduction on transport aircraft through enabling natural laminar flow on wings with high sweep and Reynolds numbers. Sustaining laminar flow on these wings has previously been limited by the growth of crossflow instabilities very near the leading edge that is common on components with high sweep at high Reynolds numbers. The CATNLF transition delay method uses carefully designed airfoils to provide specific pressure architecture that attenuates the crossflow in the leading-edge region and tailors the Tollmien-Schlichting growth to delay transition to a designated chordwise location. The method was experimentally investigated in the wind tunnel test of the CRM-NLF in 2018, and positive results

from that wind tunnel test have led to a flight test series to evaluate the CATNLF concept in a flight environment. The flight test series is comprised of three experiments, all of which have unique hardware to support the specific test objectives and will be flown on an existing testbed at the Armstrong Flight Research Center underneath an F-15 aircraft. This paper documents the aerodynamic design of the test article for the third flight of the series that is being used to evaluate the CATNLF design method.

The test article is designed to represent a typical transonic transport wing using the CATNLF design method with design conditions representing a cruise-point of Mach 0.85, Re_{MAC} of 31 million, and leading-edge sweep of 35 deg. The design is predicted to support 53% laminar flow on the suction-side of the test article and a maximum transition Reynolds number of 21.6 million on the 35 deg section. This predicted extent of laminar flow represents over three times more laminar flow, measured by transition Reynolds number, than the previous maximum seen in experimental data on configurations with comparable wing sweeps not using the CATNLF method. Off-design conditions were presented, including perturbations in Reynolds number, test article angle of attack, Mach, and test article sideslip angle, that predicts the design supports significant extents of laminar flow across a wide range of conditions.

The design was performed, flight matrix selected, and instrumentation chosen with the two primary test goals in mind: to confirm the effectiveness of the CATNLF method in attenuating crossflow growth on a representative transonic transport wing, and to investigate surface requirements needed for laminar flow applications. A potential follow-on wind tunnel test of the CATNLF test article was presented with discussion on the unique benefits and challenges this additional experiment would offer.

The finalized design of the CATNLF test article offers the potential to experimentally validate the CATNLF design method in a flight environment. The laminar flow predictions for this test article would significantly expand the potential for NLF on components previously limited by leading-edge crossflow transition.

Acknowledgments

The authors would like to acknowledge several key researchers who are critical to the CATNLF test article design effort, including Michael Frederick, Christopher Acuff, Rudolph King, and A. Neal Watkins. Additionally, the authors would like to thank the many engineers, researchers, and managers supporting this flight test at both the Armstrong Flight Research Center and the Langley Research Center. This research is jointly funded by the NASA Aeronautics Research Mission Directorate through the Advanced Air Transport Technology Project within the Advanced Air Vehicles Program and the Flight Demonstration Capabilities Project within the Integrated Aviation Systems Program. Resources supporting some computational results in this paper were provided by the NASA High-End Computing Program through the NASA Advanced Supercomputing Division.

References

[1] Boeing Company, “Commercial Market Outlook 2019 – 2038”, Website Accessed October 2019, [https://www.boeing.com/resources/boeingdotcom/commercial/market/commercial-market-outlook/assets/downloads/cmo-sept-2019-report-final.pdf].

[2] Norris, G., “Picture: Boeing plans plain grey natural laminar flow nacelles for 787s in bid to reduce fuel burn”, Flight International, July 2006, [https://www.flightglobal.com/news/articles/picture-boeing-plans-plain-grey-natural-laminar-flow-nacelles-for-787s-in-bid-to-reduce-fuel-207769/].

[3] Fujino, M., "Design and Development of the HondaJet", AIAA International Air and Space Symposium and Exposition: The Next 100 Years, AIAA 2003-2530, July 2003.

[4] Saric, W.S., Carrillo, R.B., and Reibert, M.S., “Leading-Edge Roughness as a Transition Control Mechanism”, AIAA 1998-0781, January 1998.

[5] Campbell, R.L. and Lynde, M.N., “Natural Laminar Flow Design for Wings with Moderate Sweep”, AIAA 2016-4326, June 2016.

[6] Lynde, M.N. and Campbell, R.L., “Expanding the Natural Laminar Flow Boundary for Supersonic Transports”, AIAA 2016-4327, June 2016.

[7] Lynde, M.N. and Campbell, R.L., “Computational Design and Analysis of a Transonic Natural Laminar Flow Wing for a Wind Tunnel Model,” AIAA 2017-3058, June 2017.

[8] Lynde, M.N., Campbell, R.L., and Viken, S.A., “Additional Findings from the Common Research Model Natural Laminar Flow Wind Tunnel Test (Invited),” AIAA-2019-3292, June 2019.

[9] Lynde, M.N., Campbell, R.L., Rivers, M.B., Viken, S.A., Chan, D.T., Watkins, A.N., and Goodliff, S.L., “Preliminary Results from an Experimental Assessment of a Natural Laminar Flow Design Method”, AIAA 2019-2298, January 2019.

[10] Rivers, M., Lynde, M., Campbell, R., Viken, S., Chan, D., Watkins, A., and Goodliff, S., “Experimental Investigation of the NASA Common Research Model with a Natural Laminar Flow Wing in the NASA Langley National Transonic Facility”, AIAA 2019-2189, January 2019.

[11] Malik, M.R., Crouch, J.D., Saric, W.S., Lin, J.C., and Whalen, E.A., “Application of Drag Reduction Techniques to Transport Aircraft”, Encyclopedia of Aerospace Engineering, 2015.

[12] Owens, L., Beeler, G., King, R., Chou, A., Balakumar, P., and Banks, D., "Supersonic Crossflow Transition Control in Ground and Flight Tests", AIAA 2019-1651, January 2019.
[13] Watkins, A.N., Peak, S.M., Goodman, K.Z., Frederick, M.A., and Hulgan, J.T., "Flight Test of a Resistive Heating Coating for Visualizing Flow Transition", AIAA 2020-3089, June 2020.
[14] Frink, N.T., Pirzadeh, S.Z., Parikh, P.C., Pandya, M.J., and Bhat, M.K., "The NASA Tetrahedral Unstructured Software System", The Aeronautical Journal, Vol. 104, No. 1040, October 2000, pp.491-499.
[15] Campbell, R. L., "Efficient Viscous Design of Realistic Aircraft Configurations", AIAA-98-2539, June 1998.
[16] Wie, Y.S., "BLSTA: A Boundary Layer Code for Stability Analysis", NASA CR 4481, 1992.
[17] Chang, C.L., "The Langley Stability and Transition Analysis Code (LASTRAC): LST, Linear and Nonlinear PSE for 2-D, Axisymmetric, and Infinite Swept Wing Boundary Layers", AIAA 2003-0974, 2003.
[18] Campbell, R.L. and Lynde, M.N., "Building a Practical Natural Laminar Flow Design Capability", AIAA 2017-3059, June 2017.
[19] Poll, D.I.A., "Some Observations of the Transition Process on the Windward Face of a Long Yawed Cylinder," J. Fluid Mech., Vol. 150, 1985, pp. 329-356.
[20] Watkins, A.N., Goodman, K.Z., and Peak, S.M., "Transition Detection at Cryogenic Temperatures Using a Carbon-Based Resistive Heating Layer Coupled with Temperature Sensitive Paint", AIAA 2019-2191, January 2019.